The Characterisation Of AlGaAsSb Single Photon Avalanche Diodes

Based On An Adapted Random Path Length Model For Time Evolution Comparisons.

By

D. J. Reeves
Supervisor: Dr. A. Marshall

Physics | Lancaster University

Department of Physics
Lancaster University
May 2018

Abstract

This report covers creation of an adapted Random Path Length model designed to include the time evolution of devices above multiplication breakdown. The simulation was compared against experimental values for a proposed Separate Absorption and Multiplication (SAM) structure device. Despite high current multiplication and relatively long active time the device was found to be unsuitable due to the low quantum efficiency, making photon absorption unlikely. The report concludes with the analysis of the optimal orientation for carrier injection, as well as providing some insights into the effect of ionisation coefficients. Suggestions are made regarding the further work required in order to tailor device structures to a required operational range.

Total Page Count: 39

TABLE OF CONTENTS

CHAPTER 1

INTRODUCTION

The purpose of this project was to determine whether a pre-fabricated AlGaAsSb diode could be used as a Mid-Infrared Single Photon Avalanche Diode (SPAD). If so the aim was to characterise the range at which the device would work, its response to a given bias voltage, and the time required for an incoming current to produce a notable signal. In order to do this, it was necessary to first determine an electric field profile of the device using current, voltage, and subsequent capacitance responses. Following experimental measurement of breakdown voltage and current breakdown time, a simulation was created using the Random Path Length (RPL) model of an idealised SPAD. These were compared to identify potential adaptions that could be made to improve device response. The simulation would also distinguish between the carrier evolution time - the time taken for an initial single photon to create a measurable response - and the dead carrier production times - the time before the device creates a false positive current, due to the promotion of charge carriers from within the device rather than from external sources - leading to a better understanding of the overall active time for the device.

1.1 Motivation

1.1.1 General Motivation

The Mid-Infrared (3-5μm range) is an extremely useful part of the electromagnetic spectrum, with uses in: quantum and optical communications, due to the fact that lower energy packets can traverse longer distances while maintaining the same bit rate; larger range and security in free range optical communication, due to the nature of the highly condensed beams and reduction in outside influences such as weather; increased accuracy and sensitivity in laser-based ranging systems, down to the ability to detect lower energy photon packets as well as exploiting the gap in atmospheric absorption for Mid-Infrared laser signals. Subsequently, any increase in understanding surrounding Mid-Infrared SPADs, or any development that advances the progress towards that goal, would be hugely beneficial to society and the scientific community.

1.1.2 Motivation For Project Direction

Within the Lancaster University Physics Department, there are simulations that describe avalanche photodiodes in terms of time dependence and current response below breakdown for a variable field. However, they are not able to accurately predict post-breakdown activity, which describes the stochastic nature of a device at large multiplication levels. As such, the project was effectively split into two parts; determining the experimental characteristics of a device, and the creation of a simulation capable of predicting the post-breakdown response required for a Single Photon Avalanche Diode. The experimental results would predict the suitability of a pre-fabricated device described in section 3.1.3 for mid-infrared single photon detection before comparison against the idealised simulation.

CHAPTER 2

THEORY

This section provides the prerequisite background knowledge required to understand the purpose and implications of the project.

2.1 Photocurrent Avalanche Multiplication

The mechanism that allows for the detection of low energy photons is impact ionisation, the product of which is referred to as avalanche multiplication. This process relies on the initial free carriers gaining enough energy to free an aditional electron/hole pair which can then propagate this process. For the purpose of this study, the distance required by the carriers in this process was assumed to have a 'hard dead space'. This means that the total distance traveled is a product of a 'dead space' in which the charges build up to a required threshold energy and cannot create any further pairs. Following this, the ionisation occurs at a random distance dependent upon the ionisation coefficients of that material. The ionisation coefficients are a measure of the reciprocal of the average ionisation length at a given electric field strength. A space-time diagram of this process can be found in Figure 2.1

2.1.1 Operational Modes

Avalanche multiplication can occur in two distinct modes, linear or Geiger. Linear mode occurs when the impact ionisation chain reaction requires a distance long enough, compared to the multiplication region length, that the multiplication will eventually naturally stop. It is referred to as linear-mode because there is a linear relationship between incoming photocurrent and the current response. Geiger mode, on the other hand, occurs 'above breakdown' and can cause theoretically infinite multiplication as the average distance required to create an additional free carrier pair is small enough that only external influences would quench the process. A diagrammatic explanation of the difference between linear and Geiger modes can be found in figure 2.2.

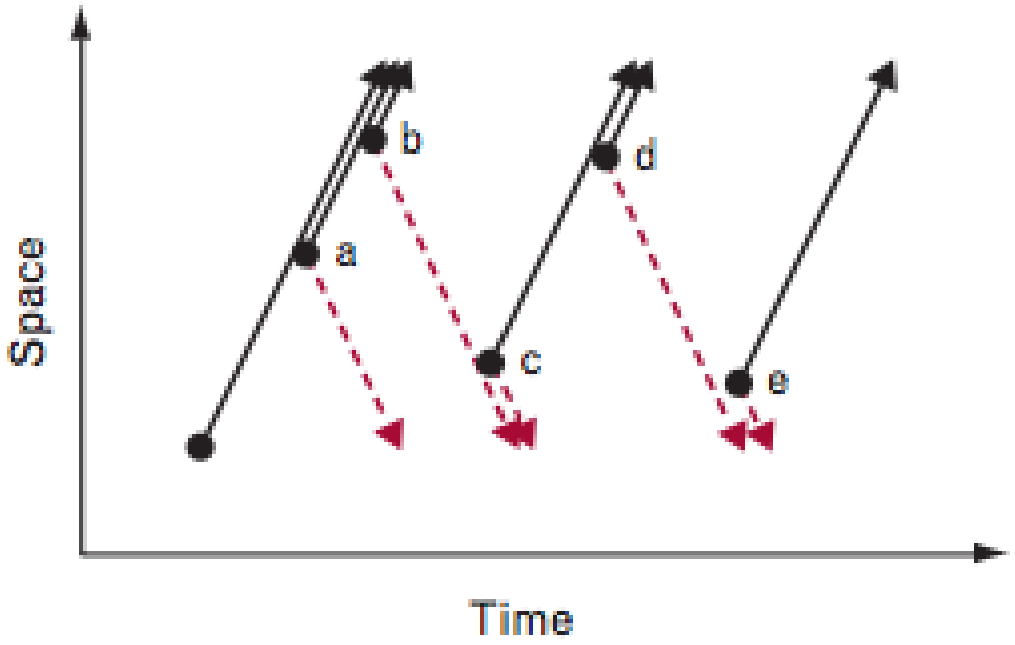

FIGURE 2.1. A space-time diagram showing the ionisation avalanche process. [2]

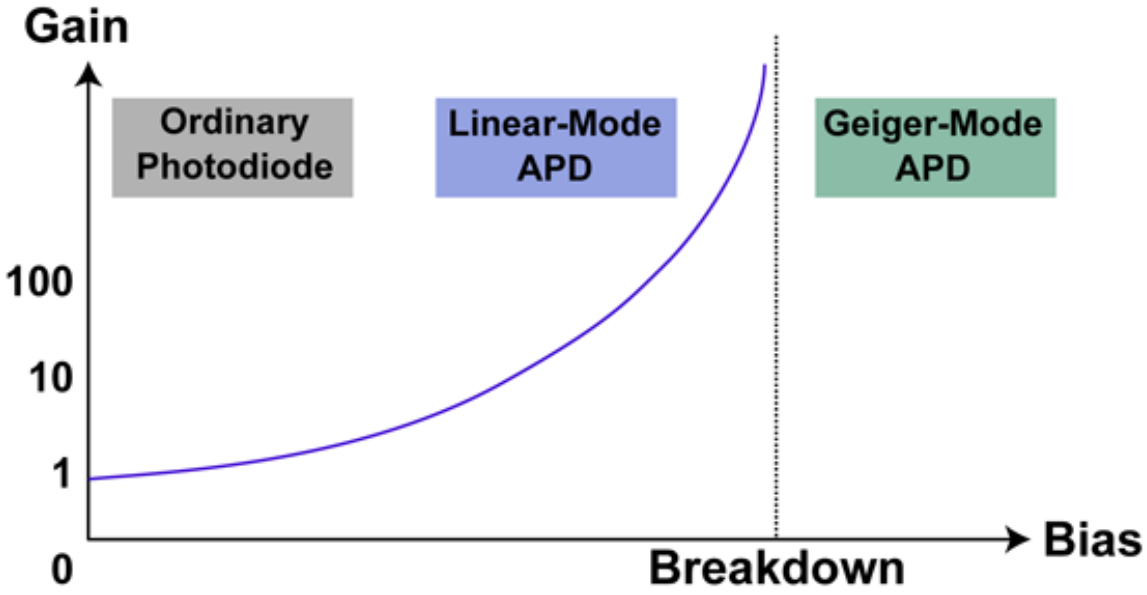

FIGURE 2.2. The characterisation of differing types of photodiode in terms of the multiplication values typically found within them.[1]

2.1.2 Ionisation Coefficients

The ionisation coefficients are, as previously mentioned, the inverse of the average distance traveled by a charge carrier and a measure of the rate at which charge carriers ionise. Within a specific material the ionisation coefficients can be modeled with an exponential dependence upon the electric field via the Chynoweth expression:

$$\alpha \text{ or } \beta = A exp\left[-\left(\frac{B}{E}\right)^{C}\right] \tag{2.1}$$

Obtained by Collins *et al*[3], the values for the ionisation coefficients and the dead space energy threshold values for the specific AlGaAsSb sample are:

$$\alpha = 1.22 \cdot 10^{7} exp\left[-\left(\frac{6.12 \cdot 10^{6}}{E}\right)^{0.671}\right] \qquad \beta = 1.22 \cdot 10^{7} exp\left[-\left(\frac{1.11 \cdot 10^{7}}{E}\right)^{0.536}\right] \tag{2.2}$$

$$E_{th\alpha} = 1.74eV \qquad E_{th\beta} = 3.38eV$$

These values are higher than other comparable materials and, as such, the device should provide higher levels of multiplication at the same field strength. As can be seen in figure 2.3:

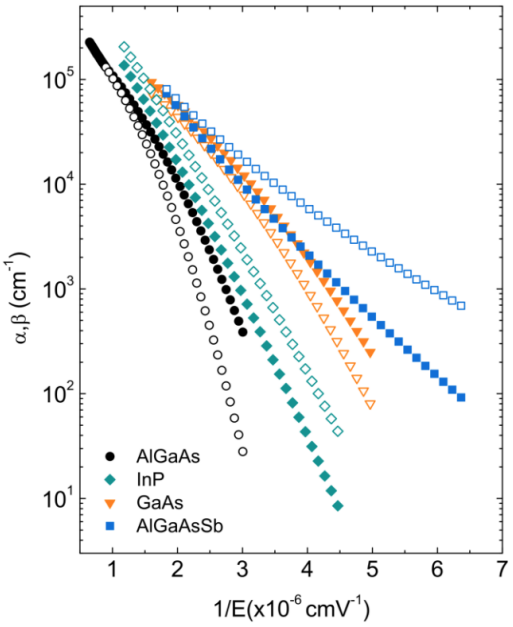

FIGURE 2.3. A comparison of the ionisation coefficients of different materials. (Collins *et al*[3])

2.1.3 Multiplication

The multiplication of a device is a measure of the increase in number of that charge carrier type. This is defined by the fraction of total charge carriers produced to the initial input of the same type. For any given trial the carrier multiplication is calculated through equation 2.3.

$$M_e = \frac{N_{e_{final}}}{N_{e_{initial}}}; \qquad M_h = \frac{N_{h_{final}}}{N_{h_{initial}}} \tag{2.3}$$

The multiplication for a given simulation is stated as the average over many trials:

$$< M >= \frac{1}{n} \sum_{i=1}^{n} M_i \tag{2.4}$$

Because the stated multiplication is an average of a number of trials, it follows that there is also a measure of the spread of the values, known as the noise, given by:

$$F = \frac{1}{n < M >^2} \sum_{i=1}^{n} (M_i^2) \tag{2.5}$$

The noise and multiplication can be used to determine roughly what response current will occur for linear-mode avalanche photodiodes based on the input current. A steep increase in multiplication and a non-linear relation between multiplication and noise can be indicative of having reached the limit of the linear-mode region and of approaching the breakdown voltage.

2.2 Device Structures

By changing dopant densities within a diode, it is possible to construct a device structure specifically aimed towards the multiplication of input currents. The gradient between dopant densities determines the electric field found across the junction between any two materials.

Typical structures for Single Photon Avalanche Diode designs are based around p-n, p-i-n and SAM junctions. p-n junctions, being the most basic design, simply provide a region of high electric field between a n-type doped material and a p-type doped material in which free charges are able to accelerate and subsequently impact ionise. Because the region of high electric field is relatively small, they are generally unable to run in Geiger-mode and so would not be suitable for a SPAD design. The same principles apply to the p-i-n diode but it includes an intrinsic, not intentionally doped, region extending the electric field and allowing for more impact ionisations to occur.

SAM designs have Separate Absorption and Multiplication regions; this structure relies on having (at least) two distinct regions within it. Initially it has a lower field region, within which carriers would not undergo much impact ionisation. The material has a specifically tailored material band gap and a high quantum efficiency for the required wavelength. This is followed by a connecting material and then a high field region with misaligned band gap. The high field region is unsuitable for photon absorption, however the previously created free carriers within

can begin a chain reaction causing large multiplication values while reducing potential noise from outside sources. The device characterised in this paper is of a SAM design, the exact structure of which is examined in 3.1.3. When a bias voltage is applied, all of these designs will typically increase both in width of the region and in electric field strength, leading to the increase in multiplication values at different voltages.

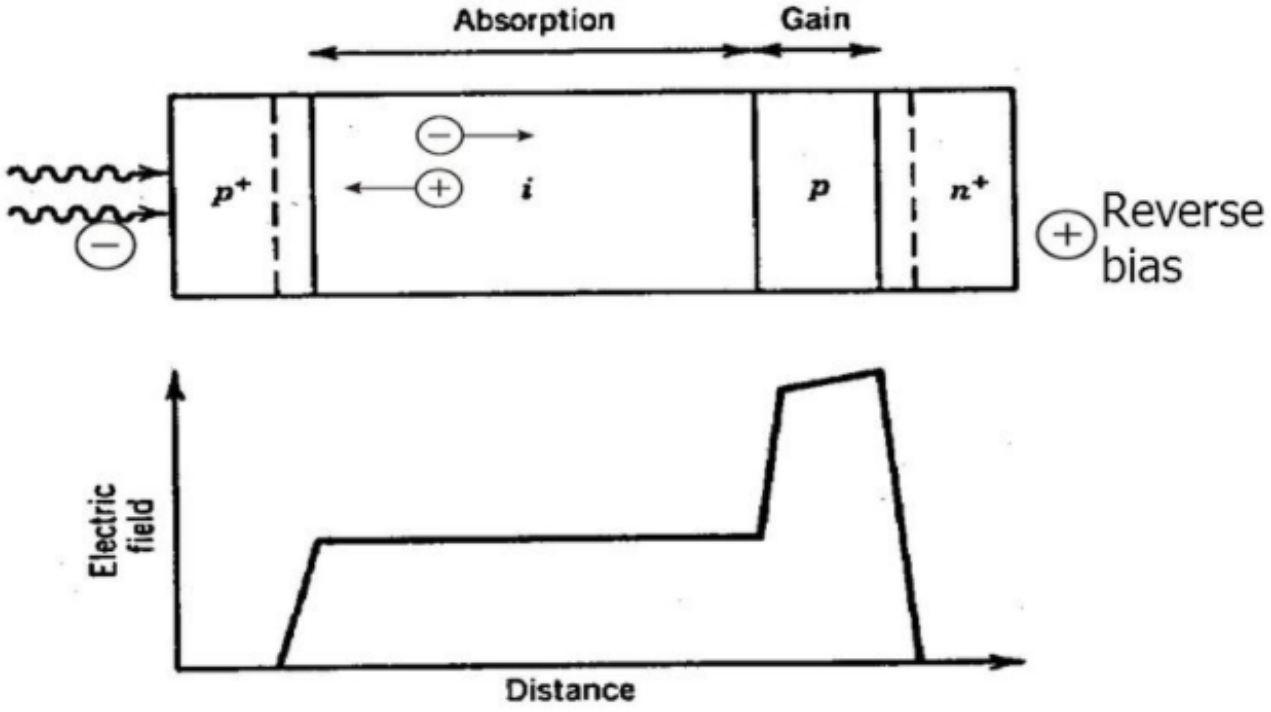

FIGURE 2.4. A schematic for a SAM avalanche photodiode. [7]

2.3 Quantum Efficiency

The quantum efficiency of the device is an important consideration during the design, a device with a low measure is unable to detect many incoming photons, therefore reducing the effectiveness of the entire device. It is defined by the ratio of number of initial carriers on the device to the incident photons. The quantum efficiency for a device can be tailored to a specific wavelength and is dependent upon both the temperature and voltage applied across the device.

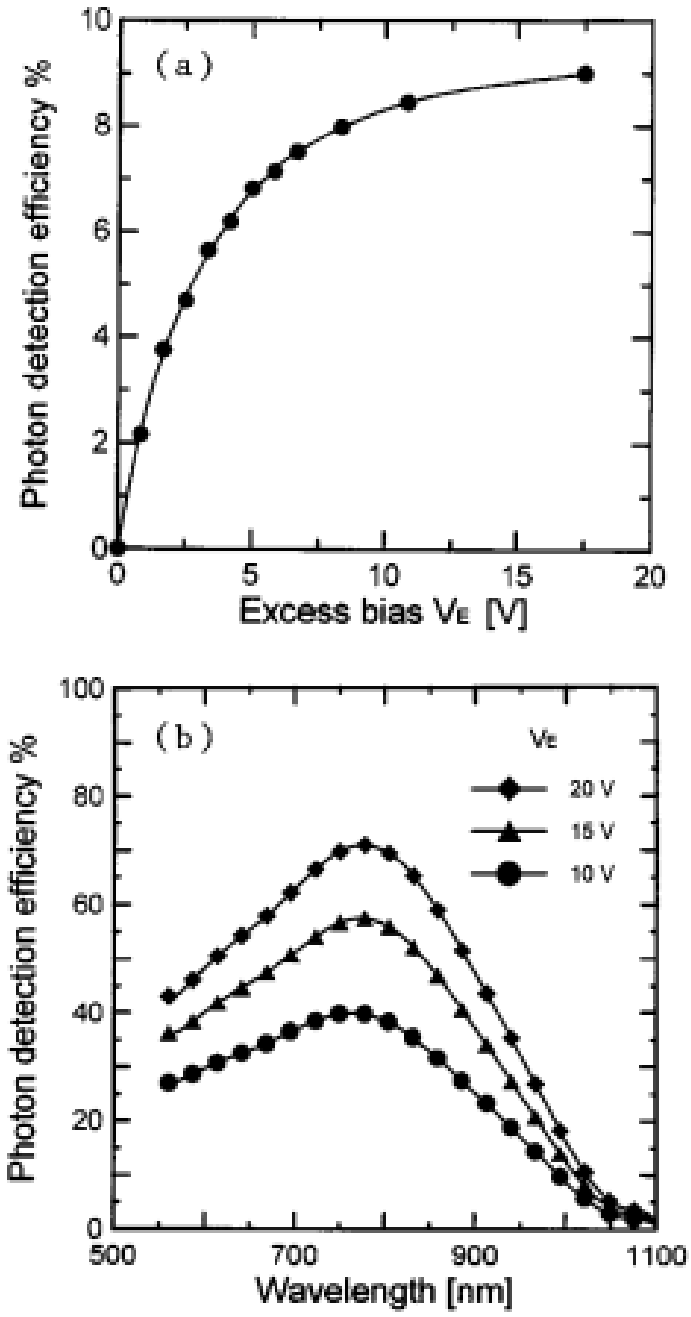

FIGURE 2.5. How the quantum efficiency of a single photon avalanche diode is effected by excess bias and wavelengths around the desired range. [4]

CHAPTER 3

EXPERIMENTAL AND SIMULATION SPECIFICS

This section provides an detailed overview of the experimental techniques used to develop a profile for the device and the principles underlying the simulation design.

3.1 Experimental Procedures

3.1.1 Current-Voltage Response

The current response provides an idea of the functional range of the device, providing an estimate of the voltages required to get accurate values in both linear and Geiger modes, as well as the breakdown point between the two. This provides an idea of the functionality of the device.

3.1.2 Quantum Efficiency

Determining the response given by any given laser wavelength and power, gives an idea of the quantum efficiency at the differing voltages, which is a critical factor in any light absorbing device. With avalanche diodes a complication is the possibility of any observed gain being due to the avalanche effect rather than absorption. The quantum efficiency can be determined by Equation 3.1 where η is the quantum efficiency, P_0 is the incoming light power and λ is the wavelength of the incoming light.

$$\eta = \frac{I_p hc}{P_0 q \lambda} \tag{3.1}$$

3.1.3 Device Structure

The device in question has a SAM based design centered around an AlGaAsSb multiplication region as is shown in figure 4.1.

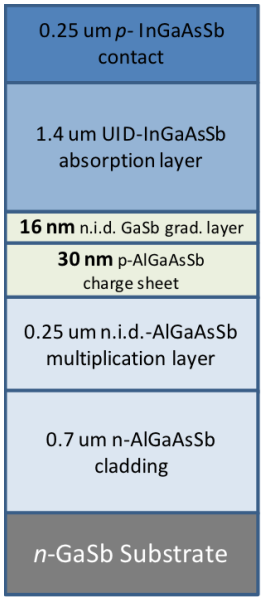

FIGURE 3.1. The device design. Please note that each of the devices were connected to a contact pad for probing on top and a general contact base at the bottom.

Using the dopant density profile it is possible to determine the field profile at different voltages as is shown in figure 3.2. These field profiles were produced using the methods outlined by A. P. Craig [5].

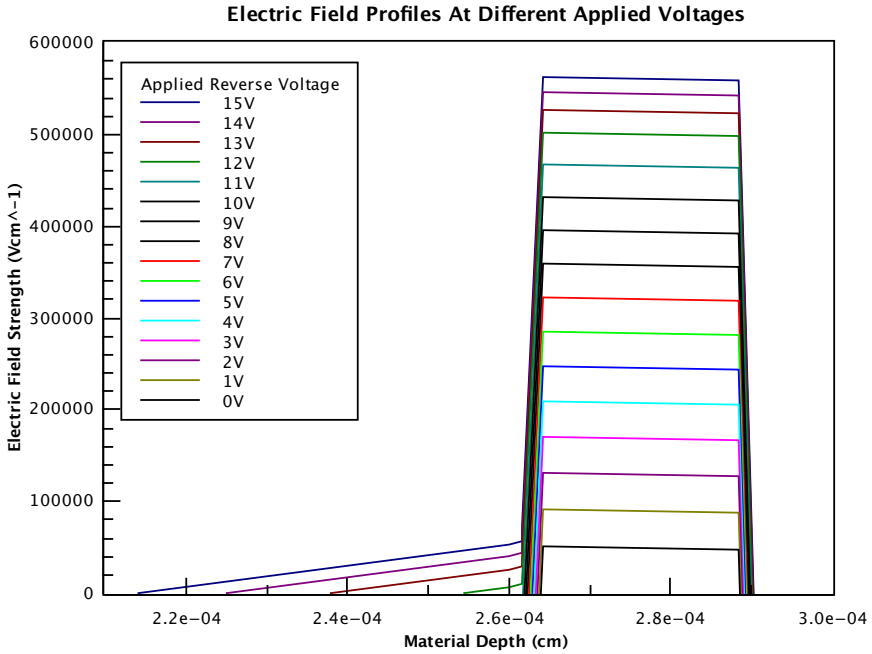

FIGURE 3.2. The field profile for the multiplication region of the device at varying voltages.

3.1.4 Dark Count Rate

While determining whether a device is fit for purpose a important component to evaluate is the time in which it is active and able to detect incoming photons, this can be quantified in part by the ‘ count rate. Due to the nature of the designs, after a certain time the device will provide a false positive current. This is due to the fact that at large enough field strengths, trapped carriers within the devices deep band structure can be promoted and behave as if there has been an incoming photocurrent. This current is then multiplied and a false response is detected. In order to quantify the dark count rate - the average time at which a false positive event will occur - the experimental setup shown in Figure 3.3 was used.

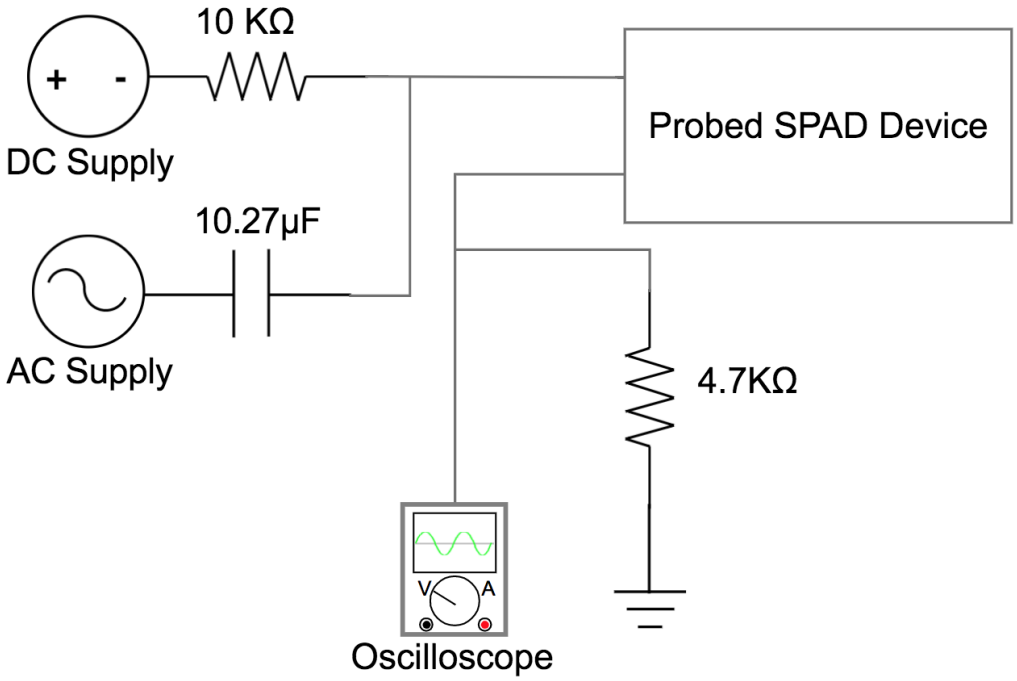

FIGURE 3.3. The experimental setup used in order to determine the dark count rate. The wiring coming into the top of the device is connected to a top probe and the wiring coming out of the bottom of the device is connected to a bottom probe.

This setup provided a combination of DC and AC voltage that could be tailored so that the device alternated between being above and below breakdown. During the time above breakdown, the dark count rate was measured and a cumulative probability distribution created. This was necessary as the dark count rate is stochastic in nature and requires an evolutionary fit to be properly quantified.

3.2 Simulation

The general simulation is based on the Random Path Length (RPL) model as set out by *Tan et al*[8]. This predicts a delay between the carrier injection/creation and first possible ionisation point. It then adapts the ionisation coefficients to account for the treatment of this delay - deadspace - as a hard boundary before which ionisation is completely impossible. The random ionisation path length of an electron x_e is described by its probability distribution function $h_e(x_e)$.

$$h_e(x_e) = \begin{cases} 0 & x_e \leq d_e \\ \alpha^* exp(-\alpha^*(x_e - d_e) & x_e > d_e \end{cases} \tag{3.2}$$

In this, d_e is the dead space and α^* is the activated ionisation coefficient for electrons. d_e is typically given by:

$$d_e = \frac{\epsilon_{the}}{qE} \tag{3.3}$$

Where ϵ_{the} is the electron ionisation threshold energy, E is the applied electric field and q is the carrier charge. α^* can be found by adapting the local equation of ionisation coefficients and is shown to be:

$$\frac{1}{\alpha} = d_e + \frac{1}{\alpha^*} \tag{3.4}$$

Using randomly distributed numbers, r, between 0 and 1 the survivability probability out to distance x_e becomes:

$$S_e(x_e) = 1 - \int_0^{x_e} h_e(x)dx \tag{3.5}$$

And subsequently, x_e can be determined as:

$$x_e = d_e - \frac{ln(r)}{\alpha^*} \tag{3.6}$$

In order to more accurately predict variable fields, the deadspace equation was adapted from that provided by Tan *et al.* [8] to account for the distance required within a linear field. The deadspace is simply the distance required to reach the threshold energy and, as such, for linear but non-constant field given by $y = mx + c$ the deadspace can be given by:

$$d_e = -\frac{mx + c}{m} \pm \sqrt{\left(\frac{mx + c}{m}\right)^2 + \frac{2 * E_{th}}{qm}} \tag{3.7}$$

In the case of a non-constant field, the ionisation coefficient part of this measurement will have to be iterated in order to maintain accuracy. In order to do this, the number of iterations is set and the simulation then calculates the activated ionisation length, multiplies it by the reciprocal of that number, propagates the particle forwards, and repeats this for the number of iterations. The ionisation coefficients are presumed to be material independent.

3.2.1 Software Design

3.2.1.1 Current Calculations

When it came to the time and current propagation of the charge carriers in the device, there were two main considerations. Firstly, if the simulation was going to give post breakdown values it would not be possible to simply follow one chain to its conclusion but rather the simulation would have to be time iterative moving all the particles at roughly the same time. Secondly, in order to be able to use the analytical deadspace calculation it wasn't possible to propagate all of the particles simultaneously. This meant that in order to find the current at any given point, it was necessary to treat the time of the particles individually.

To ensure that the simulation did not simply follow the chain of one particle, a condition was put in place so that only the lowest third chronologically would be propagated at any given loop through the simulation. In terms of the current calculation itself, it was presumed that a particle traveling half the width of the region would provide half of the current of a particle traveling the full distance of the region. Therefore, to ensure accuracy, current values could only be calculated at times before the time of the furthest back particle. To this end the following equation was used:

$$I(t) = \frac{q v_d}{w^2} \Sigma_{i=1}^{N} x_i(t) \tag{3.8}$$

Where q is the free carrier charge, v_d is the saturated carrier drift velocity (assumed to be constant throughout the device), w is the region width, N is the total number of active particles, and x_i is the distance traveled by a given active particle at the evaluated time. This is possible because, due to the constant drift velocity approximation, a particle's position is linearly proportional to the time it has been active, as such simple linear interpolation can determine the position of a particle at a given time.

3.2.1.2 Boundary Conditions

Within the device there are multiple points where the equation describing the electric field strength changes. These boundaries cause a significant complication for maintaining accuracy. The simulation deals with them in two different ways based on whether they occur during the deadspace calculation or the ionisation length calculation. The deadspace solution is simple, the energy gained so far is taken from the threshold energy and the deadspace is calculated using the new field equation. The ionisation length, on the other hand, calculates the percentage of the distance traveled so far, stops the calculation and runs it from that point. It then adds an additional iteration to the total number and, multiplies the fraction of the ionisation used for the next iteration by $1 - \%traveled$ subsequently making up for the potentially lost distance.

3.2.1.3 Simulation Hierarchy

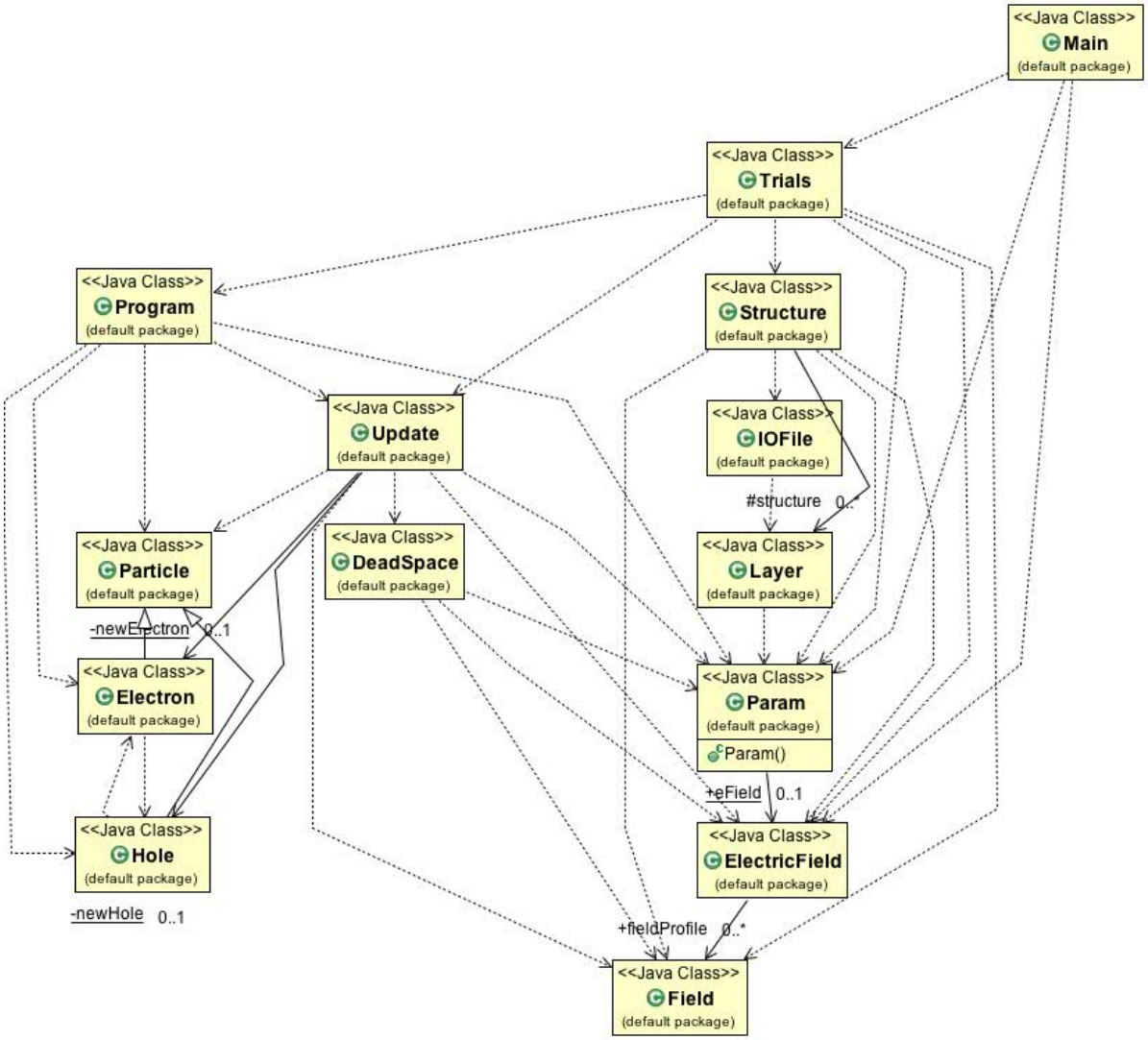

FIGURE 3.4. A class diagram of the completed simulation.

Main This is the main class for the system. It creates the Graphical User Interface and, on a button click, ensures the correct data types have been entered by the user before storing them as permanent values in the Param class. Once it has stored these values, it creates a blank electric field to allow it easy accessibility at any point throughout the simulation, and initialises the Trials class.

Trials This class is the central piece of the simulation. From here, the electric fields at differing voltages are produced and each trial is run. This class runs the program class (which handles the calculations) and subsequently sums up the multiplication values returned from each trial and is, generally, the class that will output any data requirements, unless the current evolution is being investigated.

Program This class deals with the initial carrier injection as well, as the propagation of the carriers through the junction, dealing with all the potential end conditions and necessary restrictions required.

Update The update class focuses on the iteration of a single particle. If it is the first pass through, update will simply pass the particle to the deadspace calculation class before iterating it over the activated ionisation distance. If it is not the first pass, it creates an additional electron and hole then repeats the same process for each.

Deadspace This class runs through all of the possible conditions that may affect the analytical method employed for an accurate deadspace calculation (such as the type of particle or gradient of field region), applies those that are relevant and returns the now moved particle.

Particle, Electron, and Hole These classes are simply objects that store the current position, start position, current time, and start time of a given free particle. Electron and Hole apply a boolean to the particle that is set as true for an electron and false for a hole.

Structure Structure is the object for the depletion region. It is able to take the original input file for the device structure and deplete it at differing voltages, storing this structure and outputting it, as well as the corresponding electric field, if necessary.

IOFile A class to manage the input/output file for structure related information. This is not the same input/output system that is used for the results of the simulation.

Layer This class defines the parameters for each individual layer within the depleted region. This includes dopant density, relative permittivity, and width.

Param This class contains all of the input data that may be required by the simulation. It simply stores the constant global variables that define the system.

ElectricField This class calculates field strength and gradient at any given point, as well as potentially returning which layer of the field a particle is in at a given time.

Field An object that defines the boundary points of the electric field. From these border points, all others are interpolated.

3.2.2 Proof Of Working Simulation

This section provides an estimate for the of the simulation before providing evidence to suggest that it works through comparison with results from previously validated data sets.

3.2.2.1 Variation In Values Due To Trials

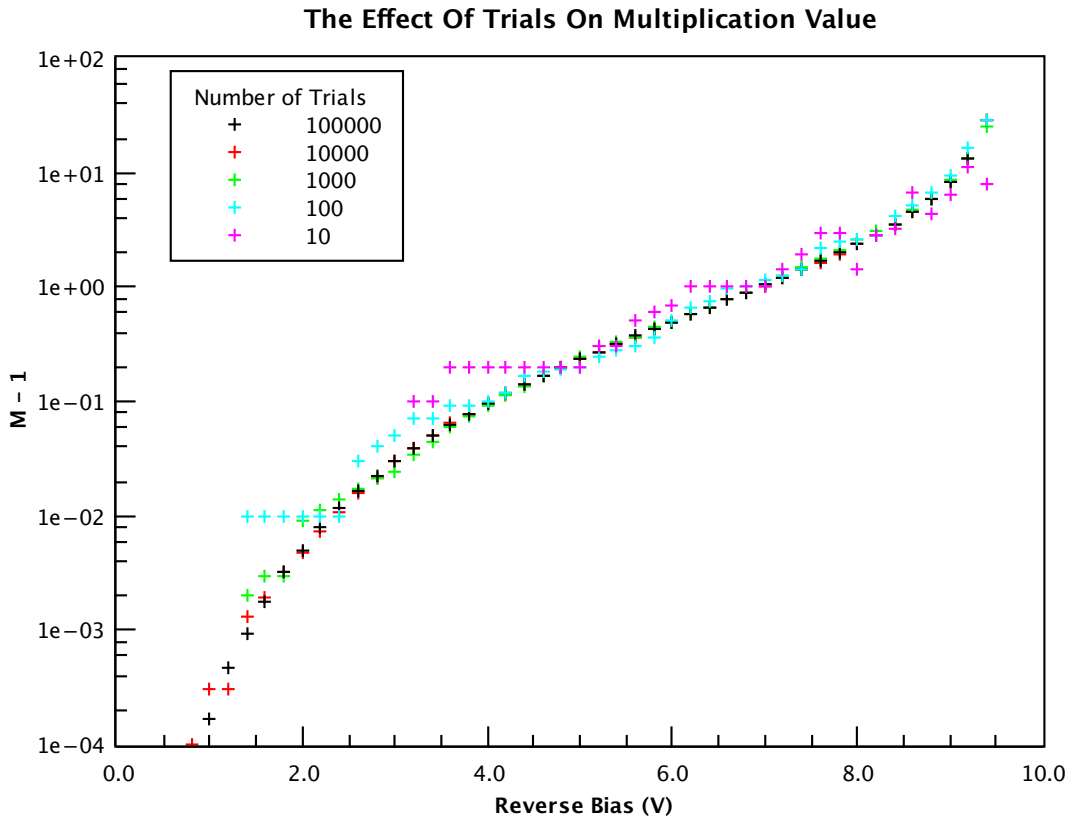

FIGURE 3.5. A comparison of how the number of trials can affect the multiplication of a simulation.

Figure 3.5 shows the effect of reducing the number of trials on a samples multiplication value. The lower the trial size, the further the values deviated from a 'true' value. In addition, the lower voltages for low trial simulations cannot be plotted as the chances of any multiplication reduces and subsequently, the chances of getting a non-zero value decreases. It can also be seen that there is a negligible determinable difference between 1000 and 10000 trials when it comes to multiplication value. As such, 1000 trials can be used as a benchmark for acceptable levels of accuracy, especially if timing is a factor.

3.2.2.2 Variation In Values Due To Iterations

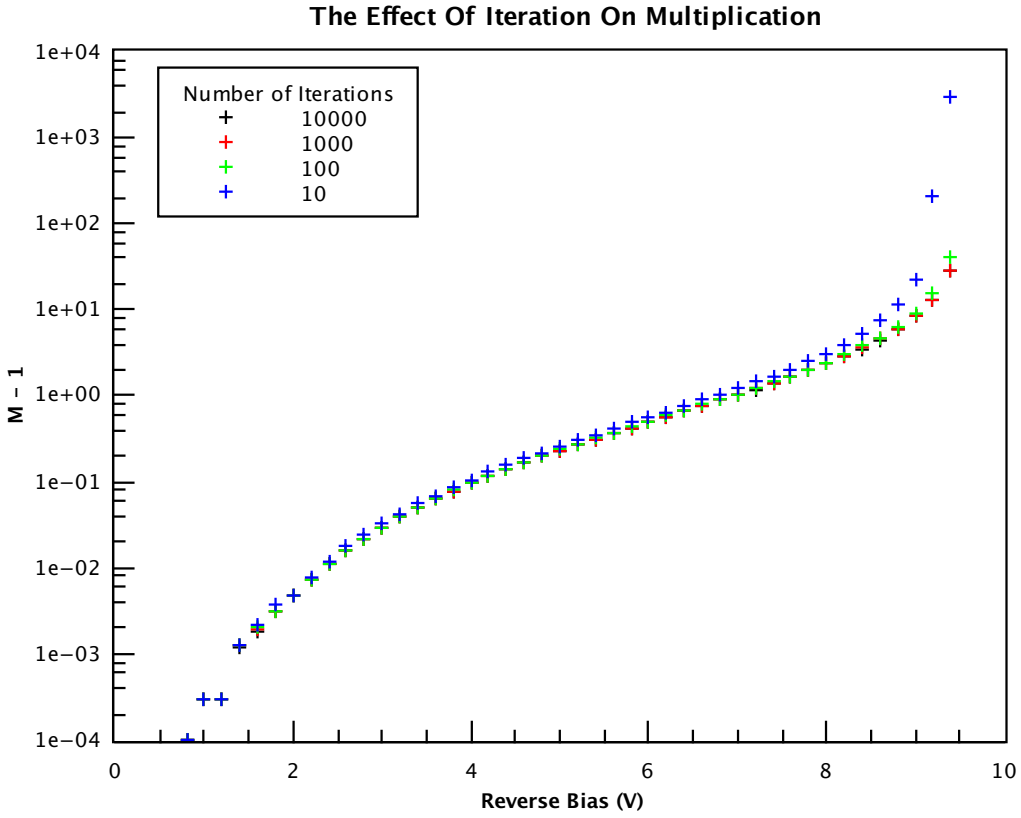

FIGURE 3.6. A comparison of how the number of iterations can affect the multiplication of a simulation.

Figure 3.6 shows the effect of adapting the number of iterations used to calculate ionisation length on a sample's multiplication value. This differs from the number of trials as, depending on the simulation setup, it either over- or underestimates the multiplication values at higher voltages. If the electric field has a negative gradient and electron multiplication is being examined then, such as in the case above, it is going to overestimate the end result. There is a less noticeable voltage effect at the lower voltage values because there is less opportunity for the lack of iterations to come into effect. At the upper end of the voltage scale, the effect becomes a lot more notable, with 10 iterations having multiplication values magnitudes above any others. From this dataset, it becomes apparent that values above 1000 iterations are indistinguishable from each other and as such, can be used as a benchmark for the minimum acceptable level.

3.2.2.3 Comparison Of Different Device Results

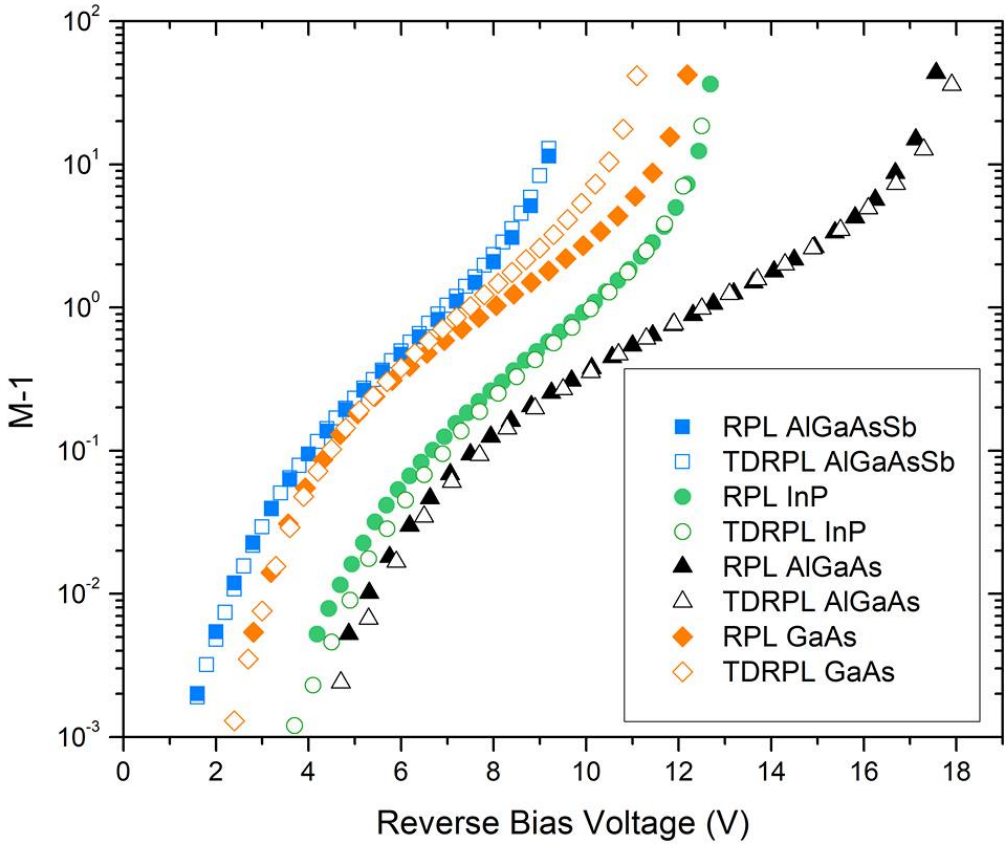

FIGURE 3.7. Comparing the Time Dependent RPL model to pre-calculated RPL model results from Collins *et al* [3]

The comparison in Figure 3.7 shows that the developed program can predict the multiplication results for a variety of materials. For the case of the GaAs results, there is an offset from those found previously that could be due to numerous reasons. Explanations include slight differences in the values used, or the way that the simulations were employed, with the RPL model from Collins *et al.*[3] being specifically tailored for accurate multiplication values. It could also be due to the number of trials/iterations employed but, as was evaluated previously, this seems unlikely.

3.2.2.4 Noise-Multiplication Relation

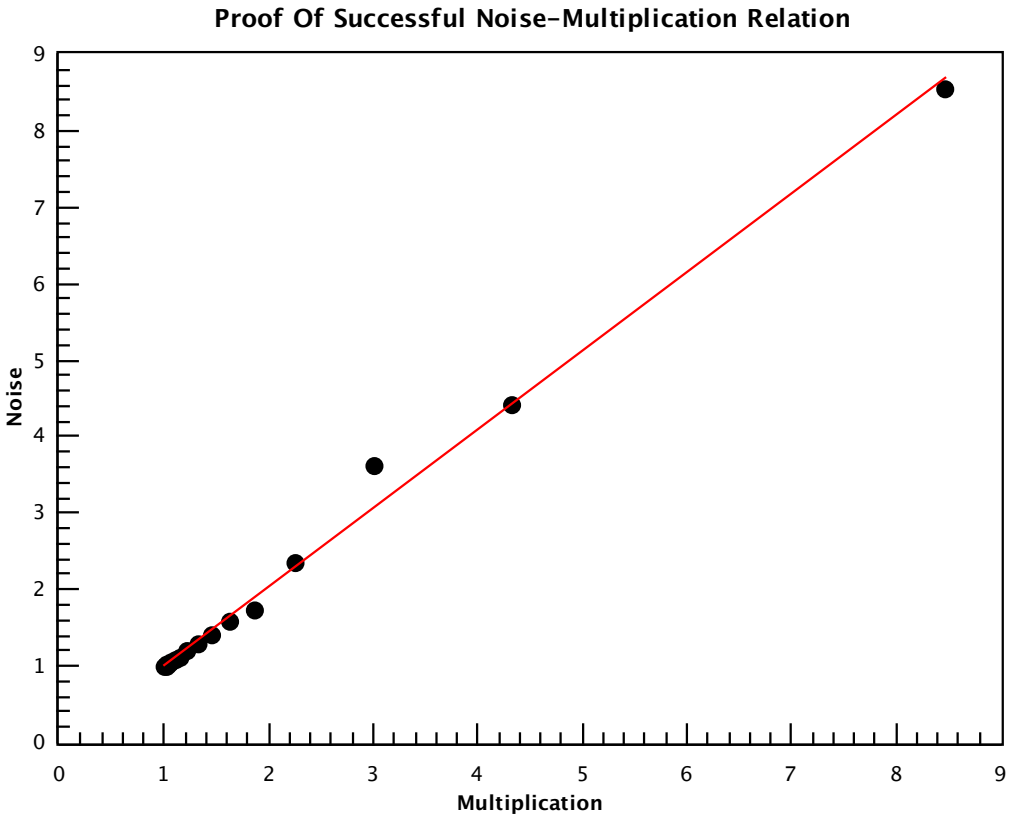

FIGURE 3.8. An example of the noise:multiplication relationship as proof of working Random Path Length model.

One of the fundamental properties of the RPL model is that if provided with no deadspace and equal ionisation coefficients (ie $\alpha = \beta$) then, below breakdown, the multiplication and noise of the system will be equal to each other. From figure 3.8 the gradient of the noise-multiplication relation is 1.03 ± 0.02 with $r^2 = 0.99$. This provides additional evidence to suggest that the RPL model has been implemented correctly. The cumulation of this section so far suggests that the simulation is accurate within the confines of the approximations used.

3.2.3 Current Evolution Of The System

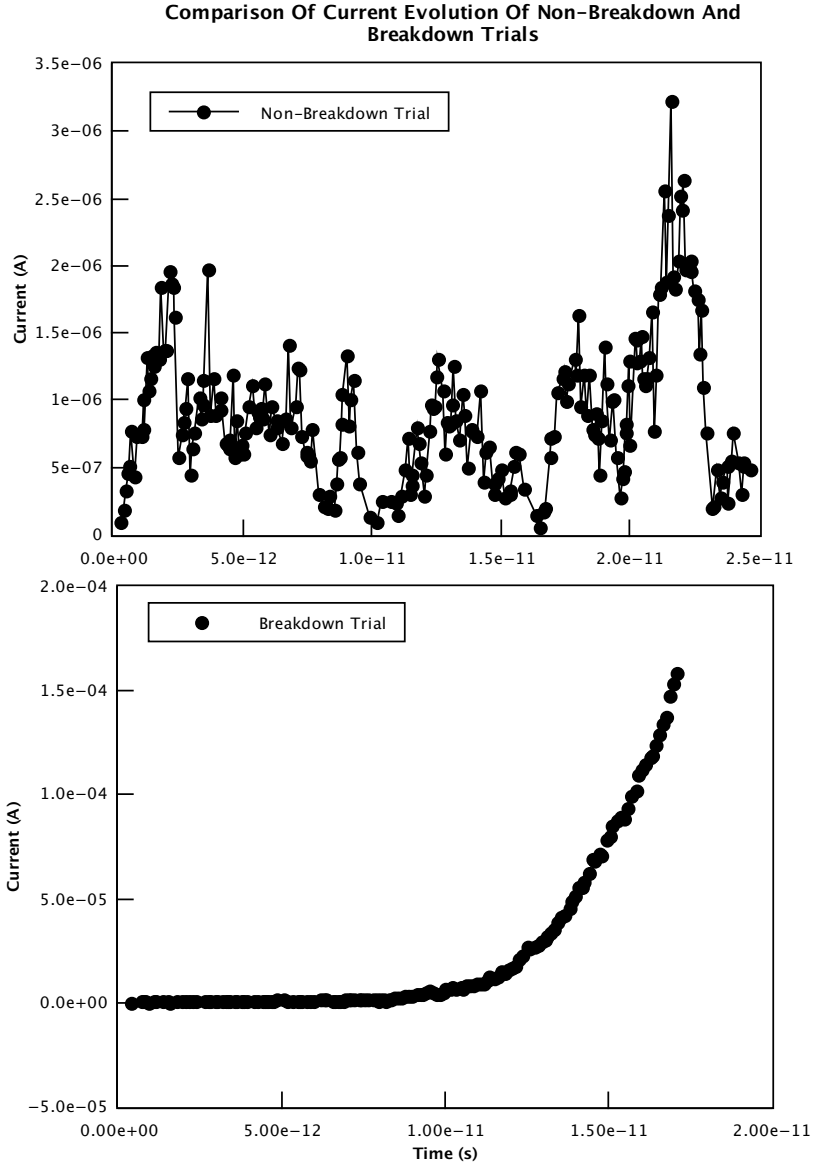

FIGURE 3.9. Current evolution graphs produced by the simulation.

Figure 3.9 shows how the current values evolve for a device below and above breakdown. The comparison shows that the current values for trials not at breakdown have a larger random element to them, as the current will typically continue to grow and fall until it reaches the point that the simulation stops as all of the active particles have left the region. Beyond breakdown, however, the current continues to grow exponentially and if a limiting factor were not put in place it would continue to do so indefinitely.

CHAPTER 4

RESULTS

This section will evaluate the experimental and simulated results. Where appropriate comparisons of the two will be made to examine whether the device would be fit for purpose. If not found to be fit for purpose, the factors that could be adapted are discussed.

4.1 Experimental

4.1.1 Voltage Response

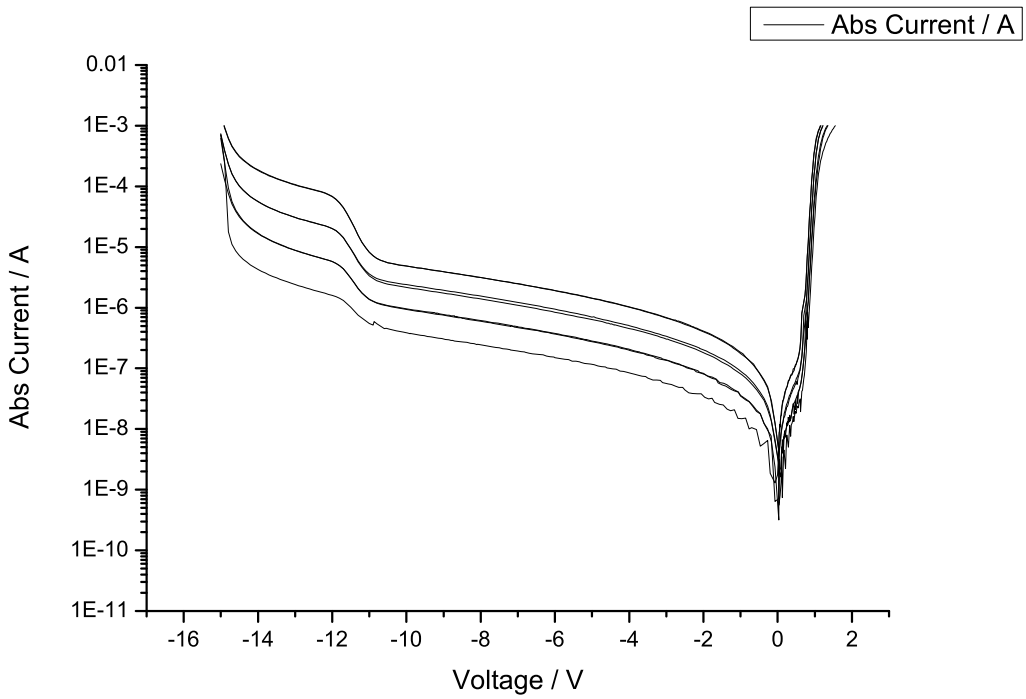

FIGURE 4.1. A comparison of the different voltage responses across differing device areas.

From the current voltage response, it can be observed that the breakdown point occurs between approximately 11.5 and 12.5 volts, this is the position of the first major uptick. As is examined in section 4.2.2 the simulated breakdown falls at around this range.

4.1.2 Quantum Efficiency

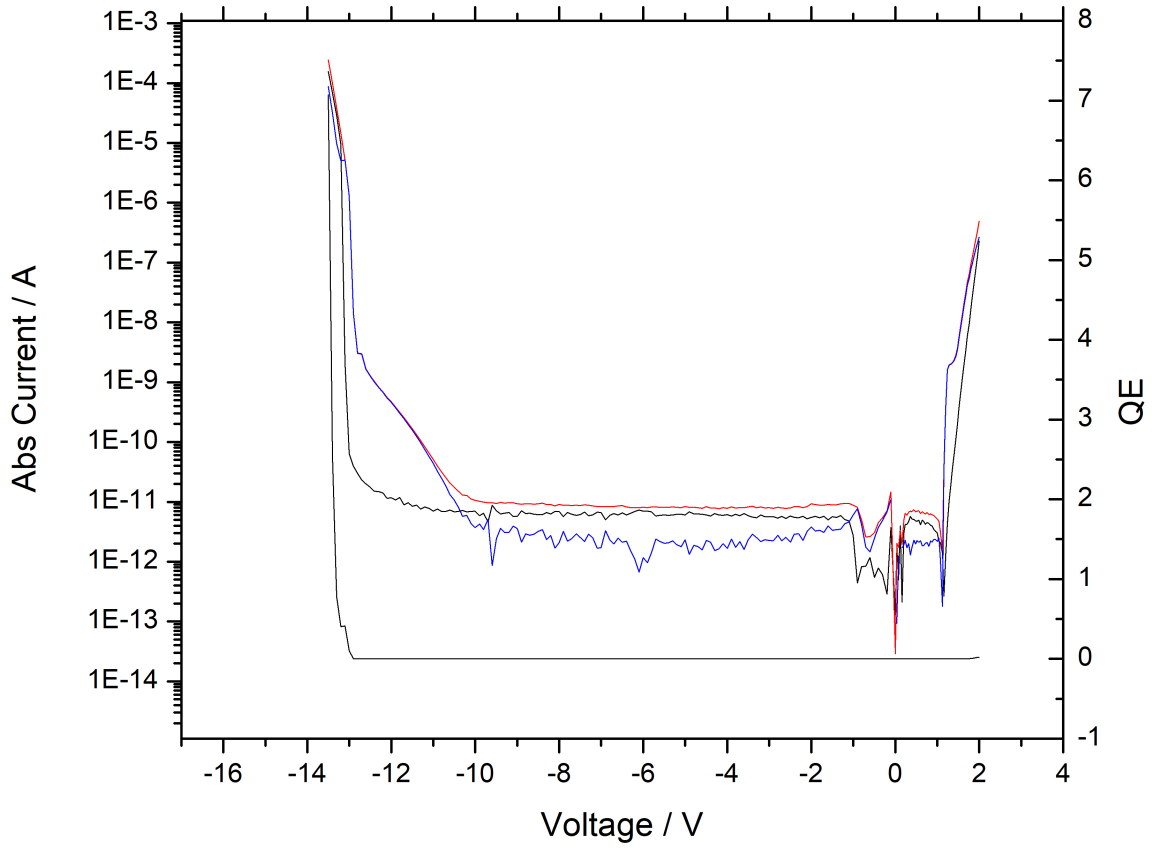

FIGURE 4.2. A graph showing the voltage effect on both current (red, blue, and higher black lines) and quantum efficiency (lower black line).

Figure 4.2 indicates that the device has a seemingly very low quantum efficiency. It's possible that the quantum efficiency increases at around $12.5-13V$ although, it is more probable that this sharp increase is due to the breakdown and subsequent high levels of multiplication. Unfortunately, this means that the devices measured are unlikely to detect the vast majority of incoming signals and as such, some part of the design, be it the absorption layer or the connection between the absorption and multiplication regions, make this device unfeasible for commercial use.

4.1.3 Experimental Dark Count Rate Measurements

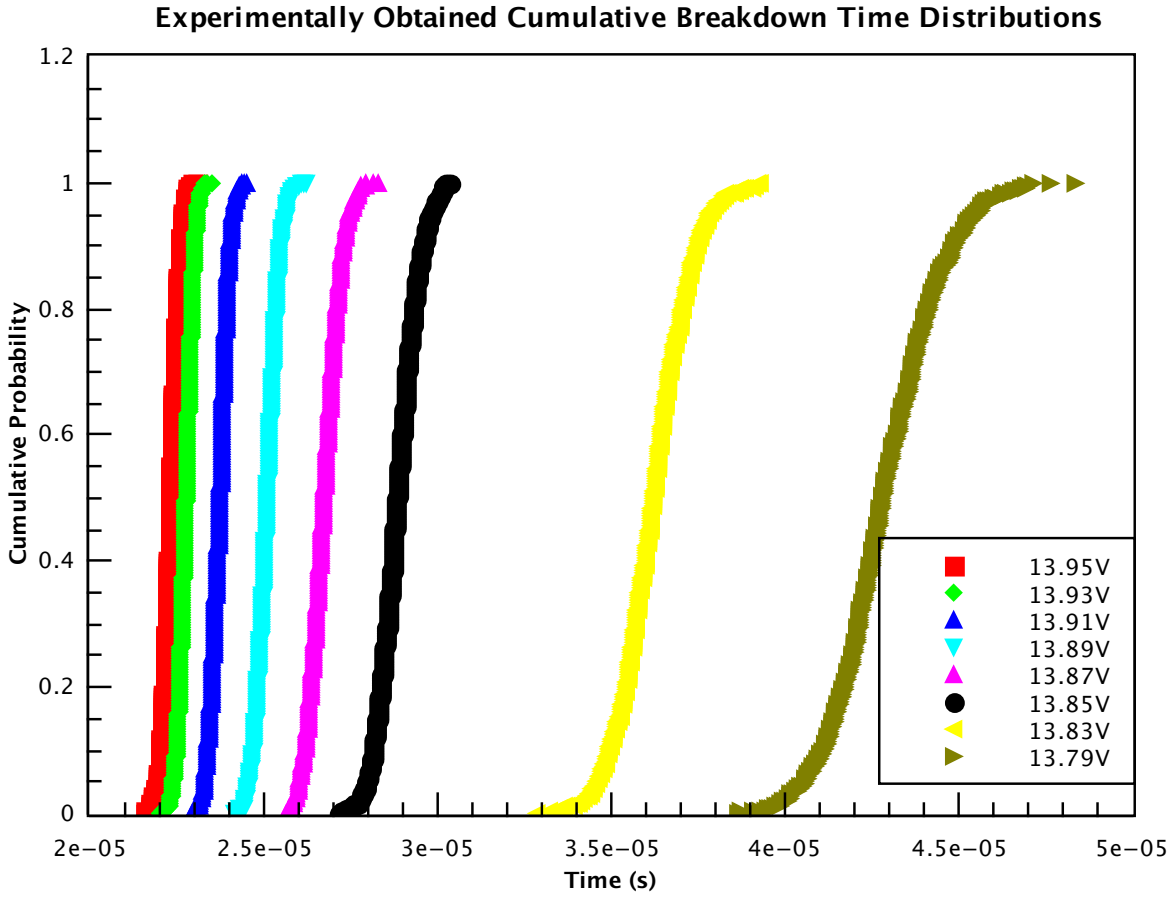

FIGURE 4.3. A graph showing the effect of α values on the average breakdown time compared breakdown probability.

By measuring the time taken for the device to produce a notable signal above breakdown while not receiving any incoming light, it is possible to estimate the dead carrier rate of the device. Due to being comprised of two distinct parts - the time required for a carrier to be promoted, and the time required for that carrier to produce a notable current response - the time required for a charge carrier to produce a notable response has been determined in section 4.2.3 of this report to better evaluate the dark carrier generation time. This process is stochastic in nature and as such, is best described probabilistically. The best fit found was a normal distribution. As well as this, the devices behave as is expected as the lower voltages take more time to reach breakdown and have a larger spread of potential values.

4.2 Simulation

The constants used in order to match the simulated and experimental results, were as described by Collins *et al* [3] and can be found in section 2.1.2. A drift velocity, assumed independent from the field strength, of $1 \cdot 10^5 ms^{-1}$ was used. This is based on the assumption of negligible difference from the drift velocity of GaAs [6].

4.2.1 Breakdown Voltage

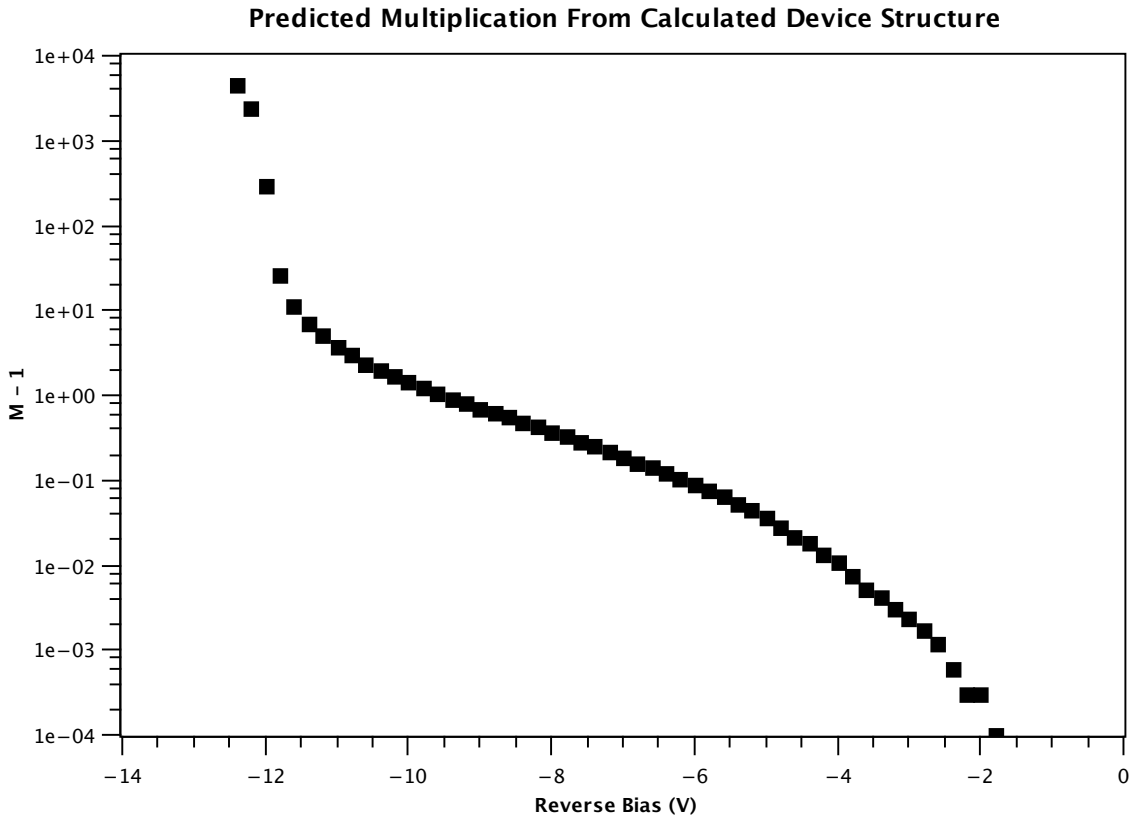

FIGURE 4.4. Multiplication values across different bias voltages for the simulated device.

From the graph, it is evident that the simulation predicts a breakdown voltage in the region of $12-12.4V$. These values are in agreement with the experimentally determined results, indicating that the process underlying the current gain within the diode is impact ionisation rather than an other multiplied signal.

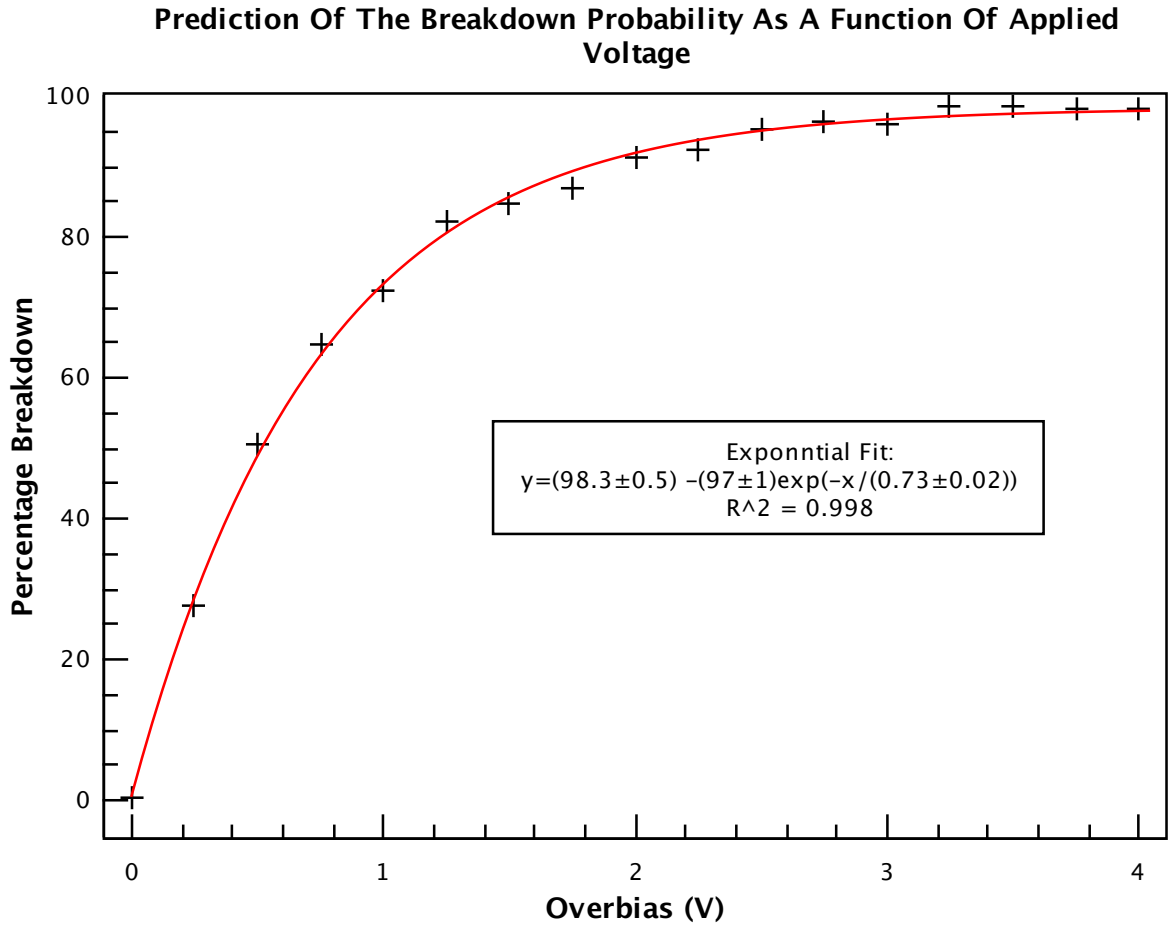

FIGURE 4.5. Shows the relation between the overbias (the voltage over a set breakdown voltage) and the breakdown probability.

Using figure 4.5, it's possible to more accurately predict the response at a given voltage. The breakdown voltage was defined as the first sign of a carrier going above breakdown. In this case, 12 V was used as it corresponds to a breakdown probability of 0.6%. Figure 4.5 indicates that the voltage at which a breakdown event happens more often than not occurs at $(12.50 \pm 0.03)V$. This agrees with both the experimental and simulated data, as a large uptick in multiplication/current response would be observable before the point of 50% breakdown probability.

4.2.2 Determining Breakdown Current

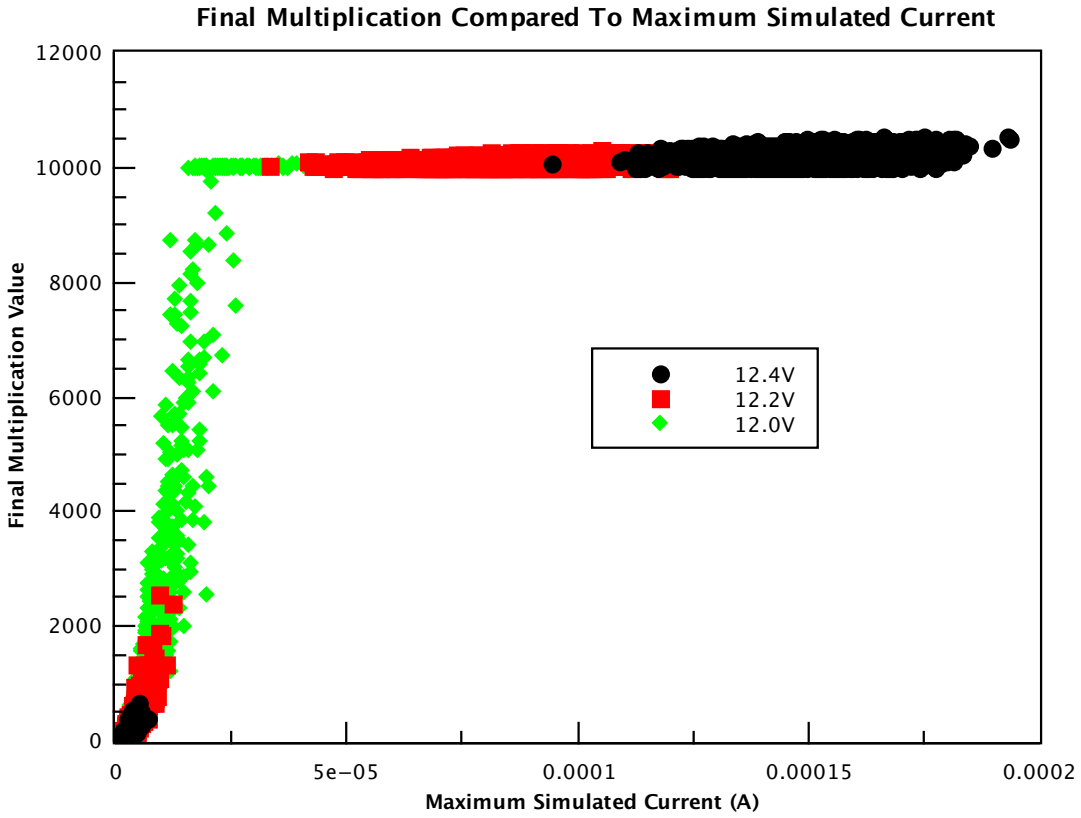

FIGURE 4.6. A plot of the final multiplication against the maximum current reached during the trial.

Figure 4.6 plots the maximum current reached in a given trial against the final multiplication of that trial. From this it is possible to see which currents didn't result in a breakdown multiplication. In this scenario, the breakdown multiplication was set to 10000. On inspection of the plotted graph, it is evident that some of the $12.0V$ points would not be broken down even past the 10000 multiplication limit. From this graph, a breakdown current limit can be set at $2.6E-5$, a value slightly above the highest non-broken down current shown. Increasing the multiplication limit would continue to provide a distinction between current values for breakdown events as opposed to non-breakdown events. A limit of 10000 provides accurate values without sacrificing large amounts of time.

4.2.3 Evaluating Breakdown Probability Distributions

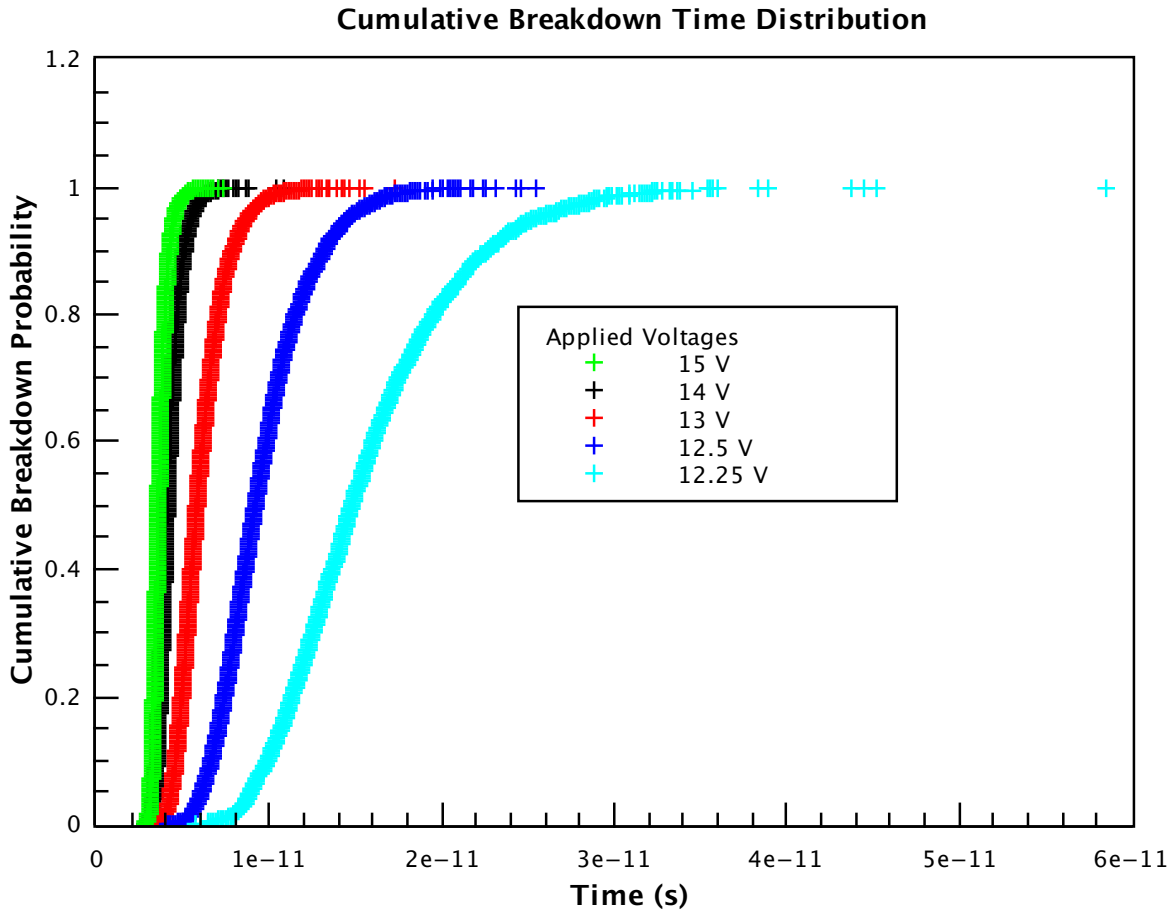

FIGURE 4.7. Cumulative probability distributions describing the time required to reach breakdown current.

Using a current limit of $2.6E-5$, it is possible to see the breakdown time distributions given different bias voltages. They appear to be poisson distributed with a minimum breakdown time of $2E-12$ and a maximum breakdown time inversely proportional to the voltage applied. The values found here are drastically different to those that were found experimentally. Not only are the current values approximately six orders of magnitude lower but, as mentioned, they are distributed according to a poisson distribution. From this, it is hypothesised that the majority of the time required for a dark count to occur is due to the chance of promoting a free carrier, rather than the build up time itself. As the current build up time for the device is effectively negligible, it is possible that at a given voltage the active time for the device before a false positive response can be seen to be equal to the shortest time perceived in the dark count rate measurements in section 4.1.3.

4.2.4 Simulated Values For The Carrier Build Up Time

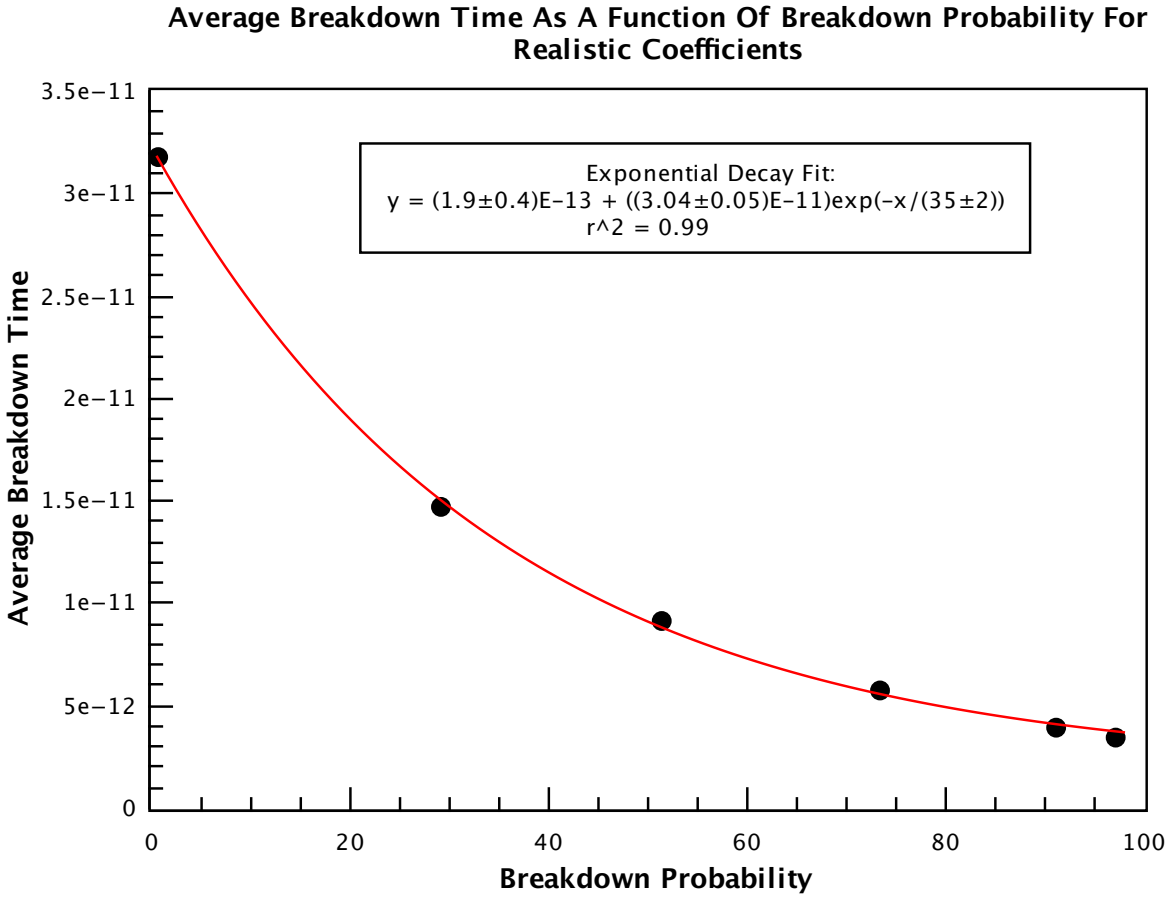

FIGURE 4.8. A comparison graph of the effect that breakdown probability has on the average time for a carrier chain to reach breakdown.

An exponential decay is the most accurate fit for the relation between the average time to reach breakdown and the breakdown probability. It is debatable whether this is in agreement with the work of Tan *et al.*[8] as no fit for their data was stated. However, both seem to fit a similar trend. If measurements of carrier response time were to be taken at different voltages using a single photon injection, the trend shown in this graph could be used to predict the breakdown probability of the device at a given voltage.

4.2.5 Predicting The Optimal Injection Orientation

Using the simulation, it is possible to predict the optimal device orientation for maximized multiplication and minimised carrier build up time. In this case four possibilities have been analysed:

1. Electron Injection with Electron Values (EIEV)
2. Electron Injection with Hole Values (EIHV)
3. Hole Injection with Hole Values (HIHV)
4. Hole Injection with Electron Values (HIEV)

The injection position describes whether the start position for the particle is in the presence of the gradual electrical field build up (electron injection) or an immediate build up (hole injection). These correspond to the injection positions of the device as it currently stands, as can be seen in figure 4.1. The values used indicate whether a hole or an electron was injected. For example, in the case of EIHV, a carrier with hole values was injected from the low field side. From these distinct situations, it is possible to determine whether the current device orientation (EIEV) is optimal or whether another would produce better results.

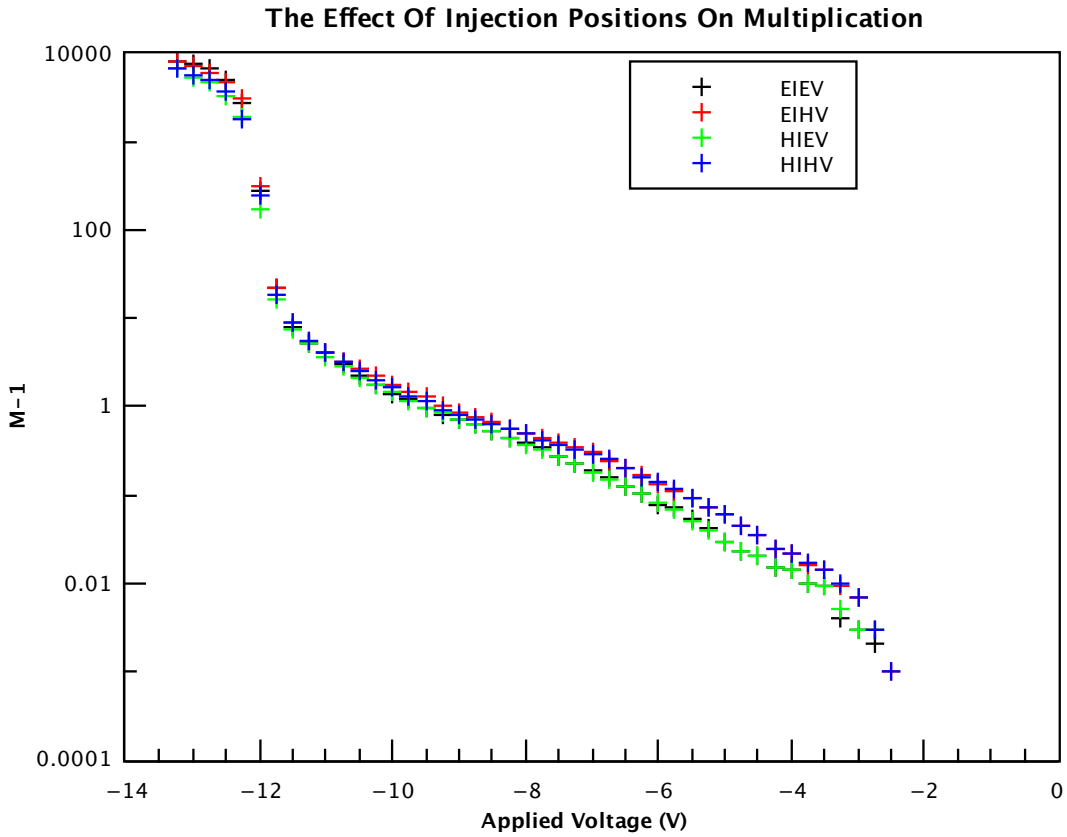

FIGURE 4.9. A comparison of the four injection possibilities on the multiplication within a device.

Figure 4.9 shows that at low voltages the main difference lies between whether a hole or an electron was injected, with holes providing a higher level of multiplication. However, at the higher voltages there is a distinct difference showing that the electron injection resulted in a better multiplication response regardless of values used. This is likely due to the initial low field that occurs at these high voltage values. Differentiating between the values used at high voltages it was found that within the electron injection scenario electrons reached a higher multiplication and that holes reached a higher multiplication than their counterparts from a hole injection. As such, when it comes to multiplication values, the current orientation of the device is optimal, at least for devices looking to be used above breakdown.

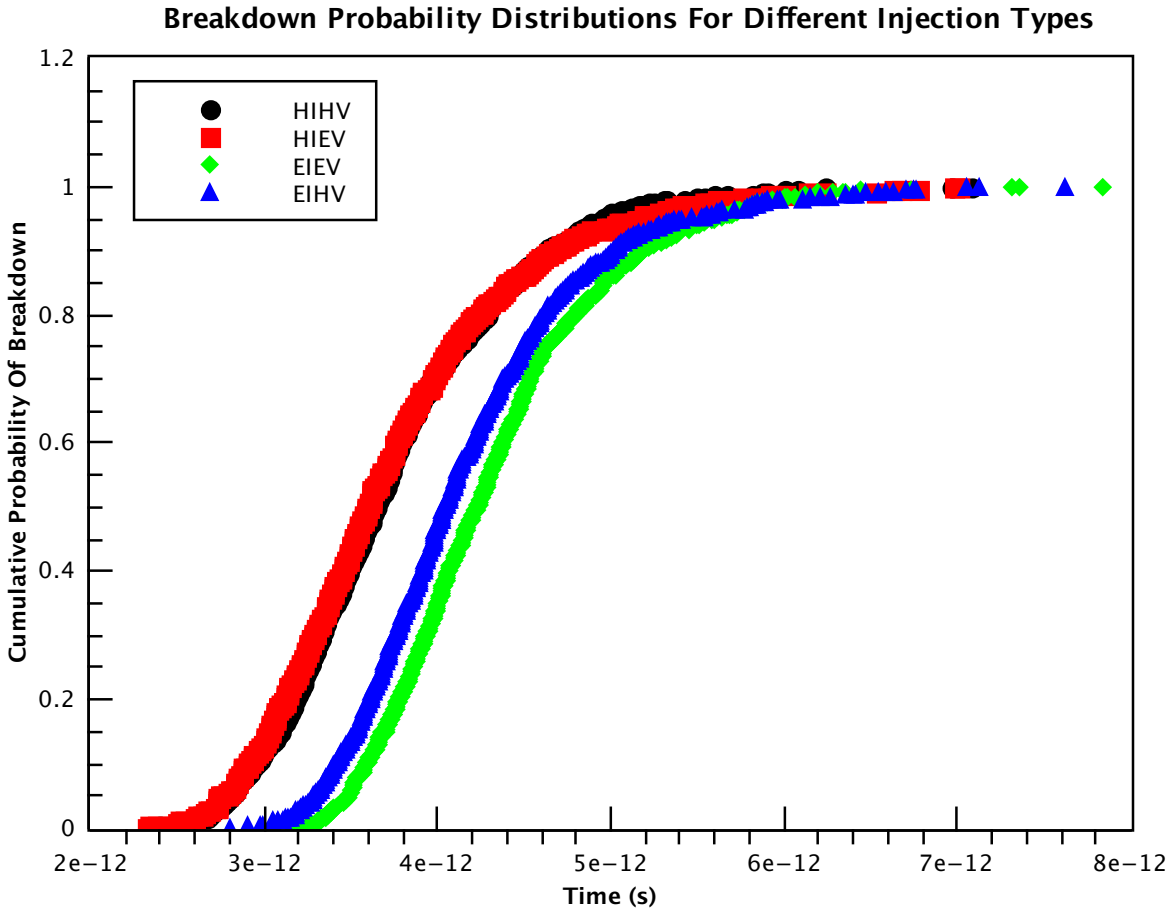

FIGURE 4.10. A graph showing the effect of the different injection possibilities on the breakdown time cumulative probability distribution.

Figure 4.10 shows that hole injections, despite having a lower multiplication (and breakdown probability), resulted in a shorter breakdown time. This means that, for the same breakdown probability as per the trend shown in figure 4.8, hole injections would reach breakdown at a substantially shorter time. In the case of the device design, this is not much of a consideration as regardless of injection position all values were still orders of magnitude lower than the current dark count rate (section 4.1.3). Subsequently, this information should only be considered relevant if dark count rate becomes a limiting factor in future device designs.

4.2.6 The Effect of Alpha Values

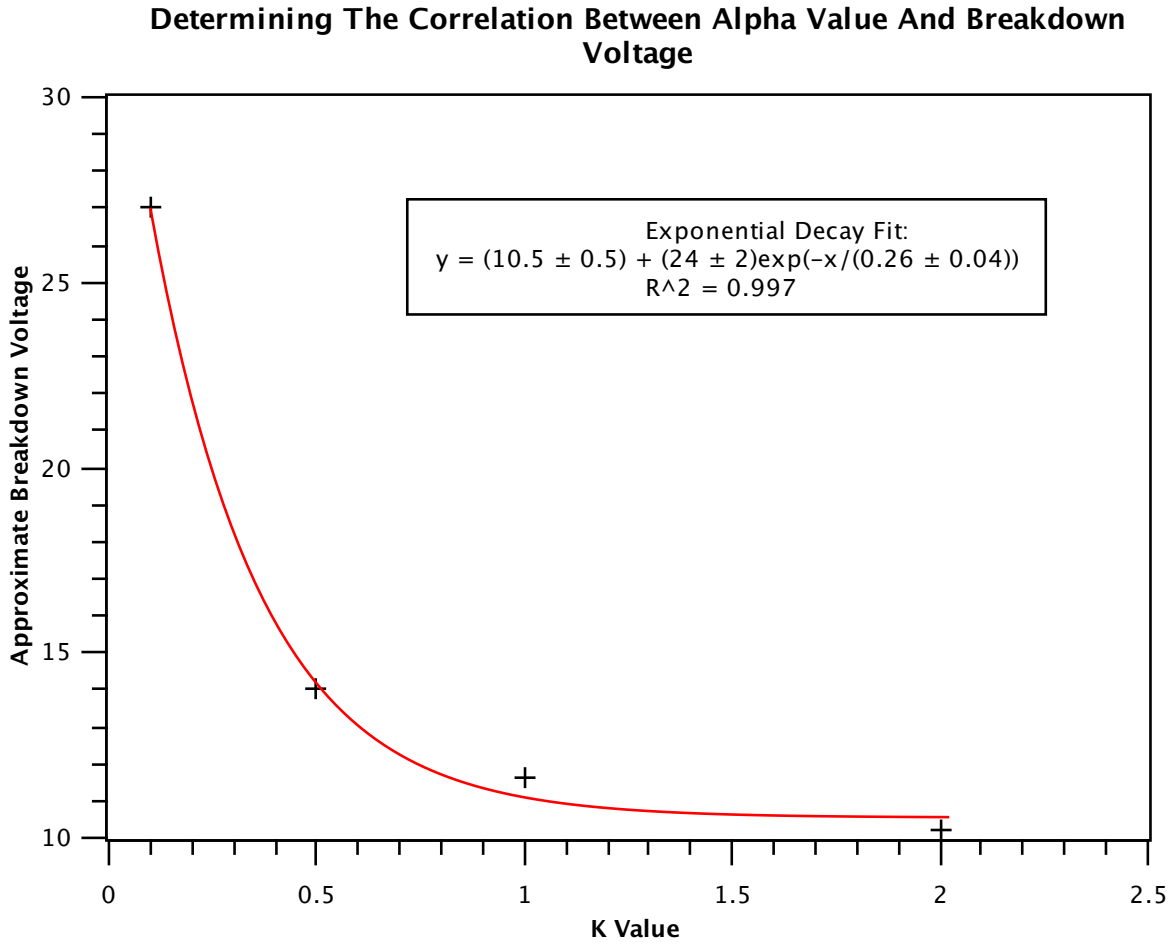

FIGURE 4.11. A graph to show the relationship between the $alpha$ value (K value) used and the breakdown voltage, defined as the first voltage in which at least one trial broke down.

Where K is defined by $K = \alpha/\beta$ and at $K = 1$, α has the previously stated hole coefficients excluding energy threshold for deadspace. Again an exponential decay was the best fit, suggesting that as the K value increases the breakdown voltage becomes asymptotic with $(10.5 \pm 0.5)V$, and that as you decrease K you find a resulting exponential increase in the required voltage for breakdown. This is in agreement with the theory outlined in section 2.1.2.

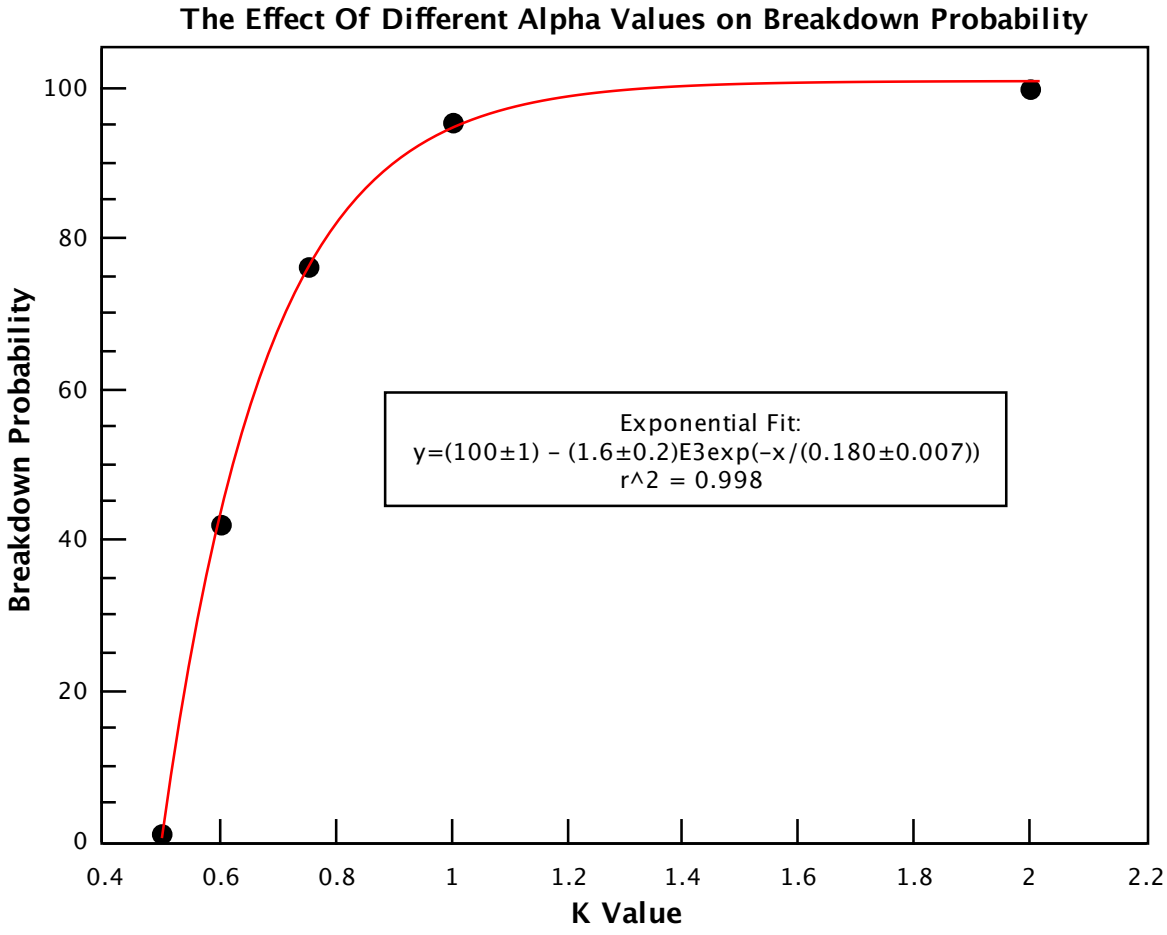

FIGURE 4.12. Graph values produced from simulations running at applied voltage values of $-14V$

Figure 4.12 provides an idea of the α values required to reach breakdown at the width of the device at 15V. This could feasibly provide an insight into the values of $\alpha \cdot Width$ required to reach a particular breakdown probability. Unfortunately, more in-depth research is required in order to accurately predict this, as the variation in the electric field strength throughout the device and subsequent variation of α^* values makes this difficult to quantify.

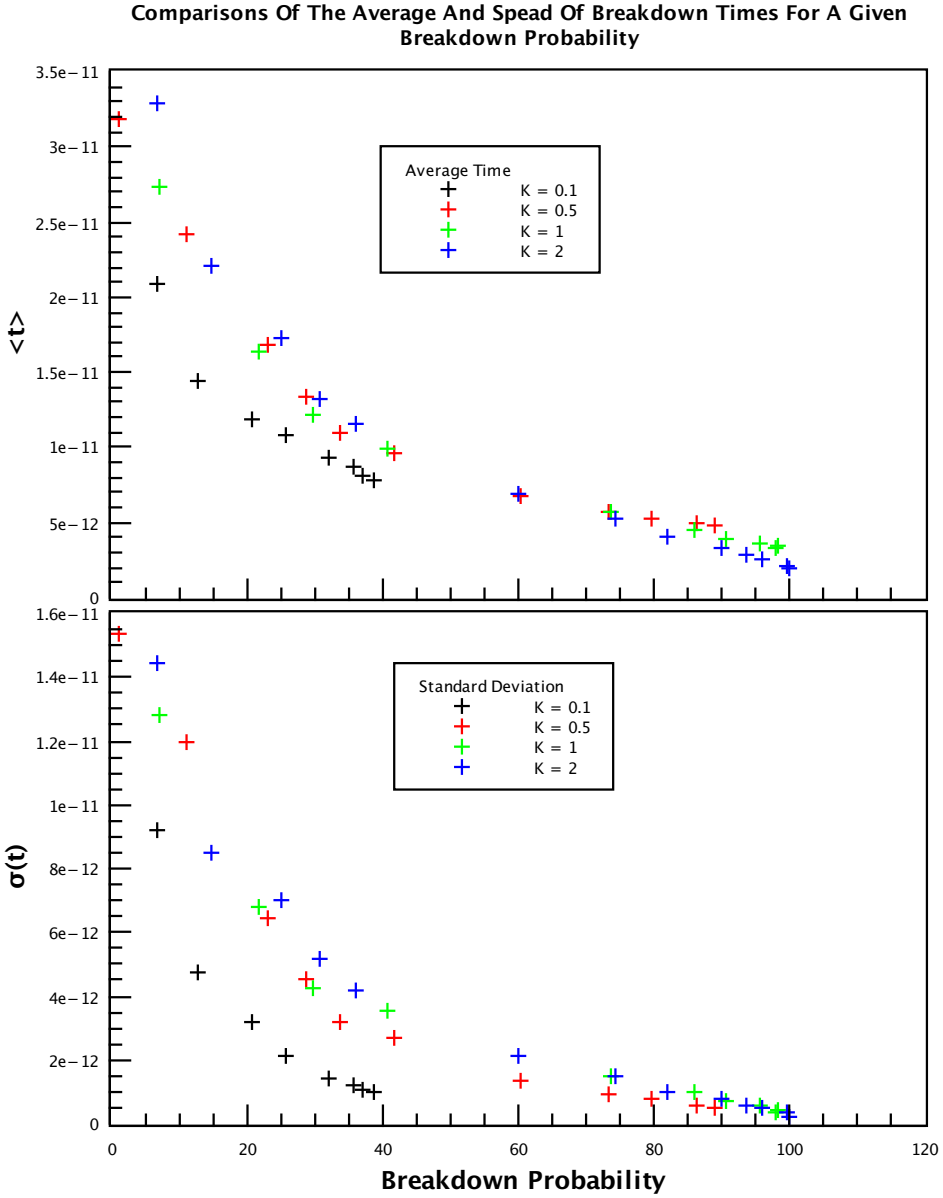

FIGURE 4.13. A comparison of the effect of α on avalanche build up time.

Unlike the data from Tan *et al* [8], the above figure shows almost no correlation between the average and spread of times at a given breakdown probability on the value of α. The apparent deviation for the values in $K = 0.1$ is likely due to the extremely large field strength required to produce the values making the dead space effectively negligible, reducing the resulting time required to reach breakdown. The larger breakdown probabilities for $K = 0.1$ were not calculated as the simulation appeared to break down and higher voltages began to predict lower breakdown probabilities; this is likely due to the value of $\frac{1}{\alpha^*}$ trending to zero as the electric field strength is increased, for fixed ionisation constants and deadspace. The general trend is that there is an exponential decay in the average and the spread of the time required to reach breakdown as breakdown probability increases.

CHAPTER 5

FUTURE WORK AND CONCLUSION

Due to time constraints, there remains potential for the simulation to predict further relationships that have not been evaluated in this report, or that could be evaluated more fully. Having proved that the simulation seemingly works successfully it should now be possible to predict values of $\alpha \cdot width$ that could influence future device designs in order to tailor the device to an approximate operational voltage for the breakdown probability required. As well as this, adaptations to the core code could be implemented. Examples include, having the ionisation coefficients be dependent upon the layer structure, allowing for adaptable saturated drift velocity measurements with electric field strength, or even moving the current calculations into a more accurate technique altogether.

5.1 Summarising Statement

The overall aims of this project were achieved. In terms of the experimental aspect, the device was found to provide suitable levels of multiplication at a functional range indicative impact ionisation multiplication and could, therefore, be considered useful for single photon multiplication. The device was also determined to have a suitably long dark count rate, in the order of $20\mu s$ at $13.95V$, corresponding to a simulated breakdown probability of approximately 80%. When compared to the carrier breakdown time, it was found that effectively all of that time was due to the dead carrier generation rate. As such, the device would have an approximately $20\mu s$ active period in which 80% of any detected photons would produce a notable current response. Unfortunately, despite the multiplication region of the device yielding promising results, the absorption and/or connection region means that it cannot be used as a functional Single Photon Avalanche Diode. The quantum efficiency of the device is effectively zero up to around the point of breakdown, above which there is a sharp uptick, presumably due to the high multiplication value of any incoming photocurrent rather than an increase in quantum efficiency itself.

The simulation created to determine post-breakdown characteristics for avalanche devices was found, under the correct parameters, to accurately predict the multiplication of a range of devices. The simulation was able to predict relations between the applied bias and the breakdown probability in line with the experimental observations. The simulation also provided an estimate of carrier breakdown times, allowing the quantification of the dead carrier generation rate.

When simulating the effect that different quantities may have on future device structures it was found that an exponential decay was the best fit for the relation between α value and the approximate breakdown voltage. Contrary to the conclusions of Tan *et al.* [8] no discernible difference in breakdown time at a given breakdown probability was found for different K values. This is likely an example of where a more realised current calculation would produce a different result due to the approximation of a constant saturated drift velocity. Finally it was determined that the optimal orientation of the device connection to the absorber, at least in terms of multiplication, was an electron free carrier injected into the low field region.

All in all the simulation has provided a strong basis for future research into the effect of single photon avalanche diode designs on overall outcomes, and has the potential to provide new insights within the department into the factors contributing to the time evolution of Single Photon Avalanche Diodes post breakdown.

BIBLIOGRAPHY

[1] *Mit lincoln laboratory: Advanced imager technology: geiger-mode avalanche photodiodes*, 2018.
Available at: https://www.ll.mit.edu/mission/electronics/ait/imaging-technology/geiger-mode-photodiodes.html.

[2] B. F. AULL, A. H. LOOMIS, D. J. YOUNG, R. M. HEINRICHS, B. J. FELTON, P. J. DANIELS, AND D. J. LANDERS, *Geiger-mode avalanche photodiodes for three-dimensional imaging*, Lincoln Laboratory Journal, 13 (2002), pp. 335–349.

[3] X. COLLINS, A. P. CRAIG, T. ROBLIN, AND A. R. J. MARSHALL, *Impact ionisation in al0. 9ga0. 1as0. 08sb0. 92 for sb-based avalanche photodiodes*, Applied Physics Letters, 112 (2018), p. 021103.

[4] S. COVA, M. GHIONI, A. LACAITA, C. SAMORI, AND F. ZAPPA, *Avalanche photodiodes and quenching circuits for single-photon detection*, Applied optics, 35 (1996), pp. 1956–1976.

[5] A. P. CRAIG, *Novel structures for lattice-mismatched infrared photodetectors*, 2015.

[6] IOFFE.RU, *Electrical properties of gallium arsenide*, 2018.
Available at:http://www.ioffe.ru/SVA/NSM/Semicond/GaAs/electric.html.

[7] A. REHMAN, *Optical detectors*, 2016.
Abailable at: http://slideplayer.com/slide/8472403/.

[8] C. TAN, J. NG, G. REES, AND J. DAVID, *Statistics of avalanche current buildup time in single-photon avalanche diodes*, IEEE Journal of Selected Topics in Quantum Electronics, 13 (2007), pp. 906–910.